

Article

# Sulfate Resistance in Cements Bearing Bottom Ash from Biomass-Fired Electric Power Plants

José M. Medina <sup>1</sup>, María Isabel Sánchez de Rojas <sup>2</sup> , Isabel F. Sáez del Bosque <sup>1</sup>, Moisés Frías <sup>2</sup>   
and César Medina <sup>3,\*</sup> 

- <sup>1</sup> Departamento de Construcción, Escuela Politécnica de Cáceres—Grado de Ingeniería Civil, Universidad de Extremadura, Instituto de Investigación de Desarrollo Territorial Sostenible (INTERRA), 10003 Cáceres, Spain; ingespisuera@gmail.com (J.M.M.); isaezdelu@unex.es (I.F.S.d.B.)
- <sup>2</sup> Departamento de Cementos y Reciclado de Materiales, Instituto de Ciencias de la Construcción Eduardo Torroja (IETcc-CSIC), 28033 Madrid, Spain; srojas@ietcc.csic.es (M.I.S.d.R.); mfrías@ietcc.csic.es (M.F.)
- <sup>3</sup> Sostenibilidad en Materiales de Construcción, Universidad de Extremadura, Unidad Asociada al CSIC, Departamento de Construcción, Instituto de Investigación de Desarrollo Territorial Sostenible (INTERRA), Escuela Politécnica de Cáceres—Grado de Ingeniería Civil, Universidad de Extremadura, 10003 Cáceres, Spain
- \* Correspondence: cmedinam@unex.es

Received: 30 November 2020; Accepted: 14 December 2020; Published: 16 December 2020



**Abstract:** To address some of the gaps in the present understanding of the behavior of new supplementary cementitious materials such as bottom ash (BA) from biomass-fired electric power plants in cement manufacture, this study explored the effect of this promising material on the sulfate resistance of the end product. Cement paste prepared with 10% or 20% (previously characterized for mineralogy and chemical composition) BA was Köch–Steinegger tested for sulfate resistance. The hydration products, in turn, were analyzed before and after soaking the reference and experimental cements in sodium sulfate to determine whether the use of the addition hastened microstructural, mineralogical, or morphological decay in the material. The 56 days findings showed that the presence of BA raised binder resistance to sulfate attack. Köch–Steinegger corrosion indices of 1.29 and 1.27 for blended cements OPC + 10 BA and OPC + 20 BA, respectively, were higher than the 1.26 recorded for ordinary Portland cement (OPC). In addition, weight gain was 20.5% and volume expansion was 28.5% lower in the new materials compared to OPC. The products resulting from the external sulfate-cement interaction, gypsum and ettringite, were deposited primarily in the pores present in the pastes. The conclusion drawn is that binders bearing 10% or 20% BA are, a priori, apt for use in the design and construction of cement-based elements exposed to sulfate-laden environments.

**Keywords:** sulfate; biomass ash; durability; sustainability; binary cements

## 1. Introduction

Growing concern in civil and building construction around concrete structure durability has spurred related industrial and technological development and progress in recent decades [1]. The second-most frequent (after corrosion) pathology that shortens concrete structure service life, and one of the most aggressive, is external sulfate attack (ESA) [2]. The resulting decay is governed by complex and, at this time, poorly understood physical, mechanical, and chemical processes [3]. Sulfate attack involves essentially four processes: transport, chemical reactions, expansive forces, and mechanical response [4].

Chemically speaking, ESA results from the reaction between sulfate ions and the hydrated (portlandite, CH; monosulfoaluminate,  $C_6A\bar{S}_3H_{32}$ ) and unhydrated ( $C_3A$ ) phases in concrete

cementitious matrices, yielding gypsum ( $\bar{C}\bar{S}H_2$ ), ettringite ( $C_6A\bar{S}_3H_{32}$ ), and sodium hydroxide (NaOH). The third, NaOH, forms in the presence of alkaline sulfates ( $Na_2SO_4$ ). Because the volume of the resulting end products is 1.2- to 2.2-fold greater than that found in the starting reagents [5], the matrix expands and cracks, increasing permeability and water ingress in structures, and consequently the rate of decay. A second effect of ESA is the steady loss of strength, weight, and cohesion in cement hydration products [6].

From the perspective of durability, the technical implications of using supplementary cementitious materials (SCMs) in cement manufacture can be summarized as: (i) lower reactivity, resulting in less heat of hydration; (ii) lower aluminate phase ( $C_3A$  and  $C_4AF$ ) content due to the dilution effect and the presence of the CH needed for the pozzolanic reaction; and (iii) pore system refinement resulting from that reaction (between the SCMs and CH), because the C-S-H gels generated settle in the pores, enhancing concrete impermeability [7–9]. In addition to these favorable technical effects, SCM use is associated with social and environmental benefits, including the reduction in natural resource deployment and the furtherance of progress in the pursuit of alternative SCMs drawn from industrial waste. The latter contributes to the institution of circular economy principles in construction and compliance with cement industry environmental commitments (lowering  $CO_2$  emissions and energy consumption, among others) [10].

Scientific community sights are presently trained on assessing agroforestry waste as a possible source of SCMs, given that  $140 \times 10^9$  tonnes of biomass waste are generated yearly [11]. The focus in that line of research has been on waste whose origin lies in: (i) agroforestry biomass consisting primarily of bagasse, rice, and to a lesser extent bamboo ash, laboratory-calcined at different temperatures [12–14]; and (ii) biomass ash or biomass bottom ash from heat and/or power plants [15–17],  $\sim 10 \times 10^6$  tonnes of which are generated yearly [18]. Research efforts in connection with the latter have consisted of analyzing the effect of using biomass ash (BA) on the mechanical characteristics of the new mortars. The findings vary depending on the origin and nature of the waste, in addition to the replacement ratio [16,19,20].

Very few papers have been published, however, on the behaviour of new eco-cements in aggressive environments (chlorides, carbonation, freeze-thaw), although replacement ratios of over 10% BA have been shown to lower resistance [21]. Blending ordinary Portland cement (OPC) with up to 20% BA has nonetheless been reported to prompt water sorptivity and a decline in swelling- and shrinkage-induced variations in volume [22]. Only one paper has been published to date on sulfate resistance in cements bearing this waste. According to the authors, Modolo et al. [23], who studied the replacement of 20% to 100% of the calcite in mortars with forestry-based BA (primarily eucalyptus) from a biomass-fired power plant, compressive strength declined and surface cracks appeared on samples exposed to a 0.1 M  $Na_2SO_4$  solution for 1 year.

Against that backdrop, the present study aims to provide scientific–technical insight into the effect of blending binders with 10% or 20% bottom ash from biomass-fired power plants on sulfate resistance in the resulting eco-cements. The mechanical behaviour, porosity, and soundness of cement pastes made with new blended cements exposed to aggressive environments for different times, and the respective microstructural changes, are explored with mercury intrusion porosimetry (MIP), X-ray diffraction (XRD), and scanning electron microscopy—energy dispersive X-ray spectroscopy (SEM/EDX) analyses.

## 2. Materials and Methods

### 2.1. Materials

The biomass ash (BA) used in this study was sourced from a Spanish electric power plant fired with non-woody + woody (eucalyptus, fruit tree, pine, etc.) biomass. The waste was collected randomly in situ at three representative heights in the airtight containers in which it was stored. At the laboratory the samples were pre-conditioned (dried and ground) and analyzed for their chemical,

physical and mineralogical characteristics, as reported in earlier papers [24,25]. The specific surface was also determined and found to be 6.63 m<sup>2</sup>/g.

The X-ray fluorescence-determined chemical composition of the BA wafer revealed that it contained ~66 wt% CaO + MgO + SiO<sub>2</sub>, ~13 wt% K<sub>2</sub>O, and ~5 wt% Al<sub>2</sub>O<sub>3</sub> + Fe<sub>2</sub>O<sub>3</sub>. According to the Vassilev et al. [26] diagram, these values are indicative of type S, subtype medium acid (MA) biomass. A net 28.2% of the silica content was found to be reactive.

The X-ray diffraction findings, in turn, showed that this material had an amorphous hump across (2 θ) angles 20° to 35°, attributable in all likelihood to amorphous silica, in addition to reflections characteristic of cristobalite and quartz. Other crystalline phases detected included sylvite (KCl), calcite (CaCO<sub>3</sub>), mullite (Al<sub>6</sub>Si<sub>2</sub>O<sub>13</sub>), hematite (Fe<sub>2</sub>O<sub>3</sub>), and microcline or orthoclase-like (KAlSi<sub>3</sub>O<sub>8</sub>) alkaline feldspars.

The EN 197-1 [27]-compliant CEM I 42.5 R Portland cement (OPC) used was supplied by a Lafarge Group plant at Villaluenga de la Sagra in the Spanish province of Toledo.

## 2.2. Blends

The new cements, stirred in a high-speed power mixer to ensure uniformity, comprised OPC blended with 10% or 20% BA. These values lay within the 6% to 20% range for cement type II/A and 11% to 35% for cement type IV/A stipulated in the aforementioned standard EN 197-1 [27]. The physical, mechanical, and chemical properties of the new cements given in Table 1 show that irrespective of the replacement ratio, they met all the requirements laid down in EN 197-1 [27] for ordinary cements.

**Table 1.** New cement physical, mechanical and chemical properties [19].

Property	Blended Cement			EN 197-1 Requirement *		
	OPC	OPC + 10BA	OPC + 20BA			
Physical	Initial setting time (min)	135	204	264	≥60	
	Expansion (mm)	0	1	1	≤10	
Mechanical	Compressive strength (MPa)	2 days	40.71	38.71	31.88	≥20.00
		28 days	68.22	67.84	58.17	≥42.50
Chemical	Sulfate oxide content (%wt.)	3.14	3.06	2.80	≤4.00	
	Chloride content (ppm)	0.01	0.02	0.04	≤0.10	
	Pozzolanicity *	-	-	Positive	Positive	

\* For type IV cements; and - This property is not required for standard.

## 2.3. Method

The OPC, OPC + 10BA, and OPC + 20BA pastes were mixed with deionized water at a water/cement ratio of 0.5 to prepare 1 × 1 × 6 cm<sup>3</sup> prismatic specimens (further to the Köch–Steinegger method), 12 each per mix, medium (sulfates or water), and exposure time. They were demolded after 24 h and subsequently cured for 21 days at 100% relative humidity and a temperature of 20 ± 1 °C (consistent with the aforementioned Köch–Steinegger procedure). Groups of 12 specimens were then soaked in an aggressive 0.3 M sodium sulfate solution (4.4 wt% Na<sub>2</sub>SO<sub>4</sub> at a liquid/solid volume ratio of 22) or deionized water as the reference at 20 °C for 14 days, 56 days, 90 days or 180 days. Known as the Köch–Steinegger method [28,29], this procedure is deemed optimal for assessing blended cement resistance to this aggressive medium because it simultaneously monitors the pozzolanic reaction and assesses most of its benefits [30].

At each test age and prior to characterization, the specimens were washed three times in deionized water to eliminate any excess salts and dried to a constant weight in a laboratory kiln at 40 °C.

Specimen flexural strength and variation in weight and length were also determined at each exposure time, and pore size distribution was analyzed in the 56 days and 180 days specimens. These microstructural studies were supplemented with XRD and SEM/EDX identification of the new components formed.

### 2.4. Instrumental Techniques

Sample mineralogy was determined on a Bruker AXS D8 (Bruker, Karlsruhe, Germany) X-ray powder diffractometer fitted with a 3 kW (Cu Ka1.2) copper anode and a Wolfram cathode X-ray generator. Scans were recorded between 2  $\theta$  angles of 5° to 60° at a rate of 2°/min. The voltage generator tube operated at standard 40 kV, 30 mA settings.

The Hitachi S4800 (Bruker, Tokyo, Japan) electron microscope used to study the morphology of the blended cement exposed to the aggressive medium for 180 days was coupled to a Bruker Nano XFlash 5030 silicon drift detector for EDX determination of the chemical composition of the samples.

Porosity was quantified on a Micromeritics Autopore IV 9500 (Micromeritics, Norcross-GA, United States) mercury porosimeter designed to measure pore diameters of 0.006 to 175  $\mu\text{m}$  and operate at pressures of up to 33,000 psi (227.5 MPa) [31].

Mean pore size ( $\emptyset_{med}$ ) was found with Equation (1):

$$\emptyset_{med} = 4V/A \tag{1}$$

where  $V$  is median pore diameter (volume) and  $A$  is median pore diameter (area).

Mechanical strength was found on an Ibertest Autotest 200/10-SW (Ibertest, Madrid, Spain) test frame fitted with an adapter for 1  $\times$  1  $\times$  6 cm specimens.

## 3. Results and Discussion

### 3.1. Mechanical Properties

According to the data graphed in Figure 1 for sulfate-soaked specimen flexural (FS) and compressive (CS) strength, the latter rose in all of the blends analyzed up to 90 days and then flattened until the end of the 180 days test period. Although flexural strength also rose in specimens soaked for up to 90 ddays in the OPC + 10 BA and OPC + 20 BA blends, the patterns subsequently diverged, with strength declining in the 10% mix after that time. In OPC, flexural strength was constant until day 56 and declined thereafter. This behavior was associated with: (i) a change in cement pore size distribution; (ii) waste pozzolanicity [25], resulting in more elastic and flexible hydration products [32]; (iii) greater degree of cement hydration [32]; and (iv) initial prestressing induced by the formation of expansive compounds prior to the onset of microcracking [30].

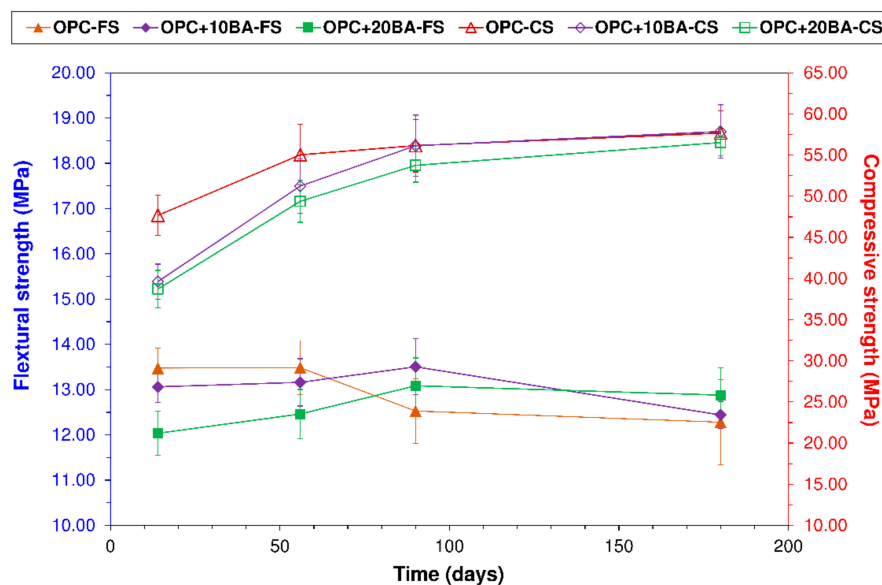


Figure 1. Mechanical behaviour of cement pastes soaked in a 0.3 M Na<sub>2</sub>SO<sub>4</sub> solution.

Figure 1 also shows that the impact of chemical attack was greater on flexural than compressive strength, as reported by Köch–Steinegger, who used this property to assess the “corrosion index” or resistance to this degenerative process [28].

### 3.2. Sulfate Resistance

Sulfate resistance was determined with the expression for corrosion index proposed by Köch–Steinegger (Equation (2)):

$$CI = F_{SS}/F_{SW} \quad (2)$$

where  $CI$  is corrosion index;  $F_{SS}$  flexural strength at aggressive sulfate exposure time  $i$ ; and  $F_{SW}$  sulfate resistance in water-soaked specimens at the same exposure time.

Further to the corrosion index found (Table 2) for the pastes studied at different exposure times, the new cements were more aggressive agent-resistant than OPC. In the Köch–Steinegger method, pastes are deemed sulfate-resistant when their 56 days corrosion index is greater than or equal to 0.70. In keeping with this criterion, the cementitious matrices designed with the new cements behaved satisfactorily when exposed to  $\text{Na}_2\text{SO}_4$ , with OPC + 10 BA exhibiting a CI of 1.29 and OPC + 20 BA of 1.27.

**Table 2.** Corrosion index at four exposure times.

Blended Cement	Exposure Time (Days)			
	14	56	90	180
OPC	1.30	1.26	1.15	1.11
OPC + 10BA	1.32	1.29	1.30	1.15
OPC + 20BA	1.29	1.27	1.37	1.19

The CI for OPC declined at longer exposure (~15%), whereas the index for the BA-bearing cements remained constant until 90 days (10% material) or rose (by ~6.2% in replacement = 20%). The 11.5% to 13.1% decline recorded after that age denoted the onset of decay.

The 56 days values for OPC + 10 BA and OPC + 20 BA were: (i) similar to those found for binary cements bearing either 15% silico-manganese slag (CI = 1.49) [33] or 20% fired clay product polishing and enameling waste (CI = 1.48) [32]; or ternary matrices with 21% paper sludge + fly ash (CI = 1.55) [34]; and (ii) lower than in pastes containing construction and demolition waste masonry materials (CI = 2.30) [35].

### 3.3. Pore Structure

The effect of 56 and 180 days sulfate soaking on the pore systems in the cement pastes analyzed is graphed in Figure 2.

Figure 2 shows that total porosity was greater in the BA cements than in OPC due to the intrinsic impact of the new addition on pore structure. This effect has been reported in earlier studies on cement pastes containing other pozzolanic materials, such as slag, fly ash, or silica fume [36,37]. Total 56 days porosity (20% to 24%), for instance, was similar to the values observed by Frías et al. [33] for matrices bearing 5% or 15% silico-manganese slag, or Sánchez de Rojas et al. [32] for cementitious systems with 20% masonry product sludge.

Total porosity declined with exposure time in all of the cements, by 6.8% in OPC, 9.9% in OPC + 10 BA, and 10.7% in OPC + 20 BA. The steeper decline in the BA-bearing cements was associated with their pozzolanicity [19], and the precipitation of expansive compounds such as gypsum and ettringite in the pore system [38]. The combined effect of those two developments was lesser permeability and a delay in decay [37,39], as attested to by the corrosion index values listed in Table 2.

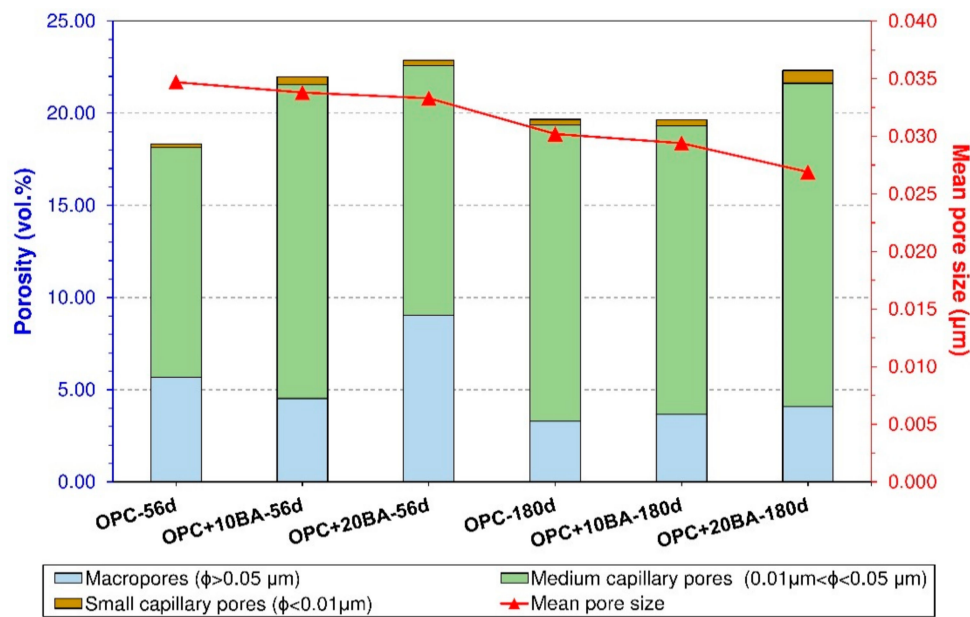


Figure 2. Pore system properties in cements soaked in a 0.3 M Na<sub>2</sub>SO<sub>4</sub> solution for 56 or 180 d.

Further to Figure 2, between days 56 and 180, pore size declined with longer exposure time, by 13.0% in OPC, 13.5% in OPC + 10 BA, and 19.2% in OPC + 20 BA. This finding was related to the inside-pore precipitation of the new compounds and BA pozzolanicity, which improved the matrix pore structure by reducing the volume of macropores and raising the fractions of medium (0.01 µm to 0.05 µm) and small (0.002 µm < Φ << 0.01 µm) capillary pores.

### 3.4. Soaking-Induced Mass and Size Changes

Weight was observed to rise over time in all of the specimens soaked in sulfates (Figure 3), 1.7-fold in OPC, 2.2-fold in OPC + 10 BA, and 2.7-fold in OPC + 20 BA cements.

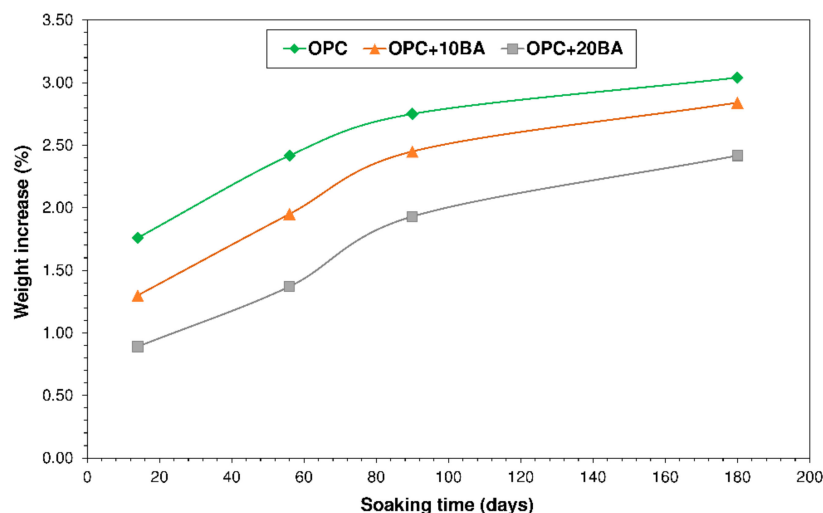


Figure 3. Variation in weight with time soaked in Na<sub>2</sub>SO<sub>4</sub>.

The increase in weight was calculated with Equation (3), where: ΔW is variation in weight in %; m<sub>0</sub> water-cured sample weight at time i; and m<sub>i</sub> weight at exposure time i (ti = 14, 56, 90, or 180 d).

$$\Delta W = [(m_i - m_0) / m_0] \cdot 100 \tag{3}$$

Weight gain induced by sulfate attack was more accentuated during the early weeks of hydration ( $t < 56$  days), after which it tapered due to declining cement paste permeability. The latter was a direct result of secondary ettringite and gypsum formation prompted by the interaction between cement hydrated phases and external sulfate ions entering the pore system [40]. Weight gain was consistently greater in the BA-bearing than in the BA-free cements at all of the times studied, perhaps due to the higher porosity in the former.

The variation in length with time of exposure to  $\text{Na}_2\text{SO}_4$  in the cements analyzed (plotted in Figure 4) revealed that weight gain (Figure 3) was attendant upon expansive product formation during sulfate penetration [41]. Inasmuch as the products occupied more space than the reagents, such crystallization was followed by expansion, cracking, and surface spalling.

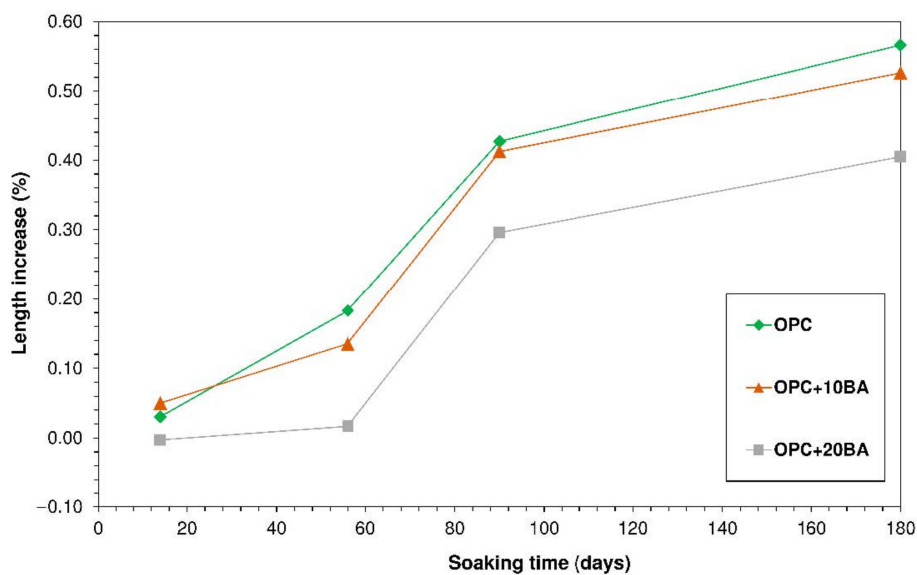


Figure 4. Expansion in cements exposed to  $\text{Na}_2\text{SO}_4$ .

The curves in Figure 4 followed a pattern observed by other authors, who divided expansion into two periods: initial or induction characterized by “steady, slow” or “progressive” expansion (up to ~56 days) followed by a stage with a “sharply” or “rapidly” increasing rate of phase expansion that proceeded until the sample disintegrated entirely [42,43].

Finally, the graph also indicates the expansion was less intense in the blends containing BA than in the reference OPC, by 7.1% in OPC + 10 BA and 28.5% in OPC + 20 BA. This behaviour might be related to the presence of larger pores and greater connectivity in the blended materials, which would favor first-stage ion transport toward macropores and concomitant crystal formation in their more thermodynamically stable interiors [44], ultimately mitigating expansion. As Ikumi et al. [38] contended, the greater total porosity in the new pastes may have a beneficial long-term effect by enhancing these materials’ capacity to accommodate precipitates generated during exposure.

### 3.5. Composition and Microstructural Analysis

The 180 d XRD patterns for OPC, OPC + 10 BA, and OPC + 20 BA soaked in water or  $\text{Na}_2\text{SO}_4$  (reproduced in Figure 5) confirmed the presence of ettringite and portlandite, the hydrated phases normally identified in cements. Unreacted BA (i.e., quartz) and calcite resulting from the carbonate formed when carbon dioxide dissolved in the solution were also detected in the blended pastes [45]. The reflections for ettringite and gypsum, the two products primarily associated with sulfate attack, were more intense in the samples exposed to sulfates for 180 days. These findings were consistent with earlier reports for Portland cement pastes [46], pastes bearing blast furnace slag [47], and cements prepared with granite sludge [29].

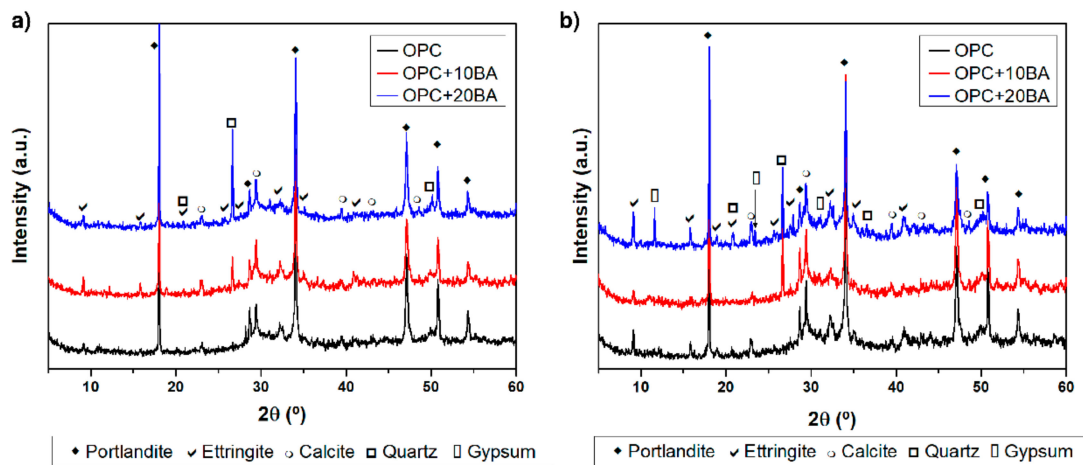


**Figure 5.** XRD patterns for pastes of ordinary Portland cement (OPC), OPC + 10 bottom ash (BA), and OPC + 20 BA soaked for 180 days in (a) water or (b) a 0.3 M  $\text{Na}_2\text{SO}_4$  solution (from the bottom to the top: OPC, OPC + 10 BA, and OPC + 20 BA).

The secondary electron (SE) SEM micrographs for the OPC and OPC + 20 BA pastes soaked in  $\text{Na}_2\text{SO}_4$  for 180 days reproduced in Figure 6a,b attest to the microcracks resulting from the generation of internal stress ( $\epsilon_{\text{local}}$ ) higher than the tensile strength ( $\epsilon_{\text{macro}}$ ) of the matrix. Such fissures appeared in stages 3 and 4 of the mechanism proposed by Santhanam et al. [42] to describe sodium sulfate attack in mortars. As noted earlier, these circumstances are the result of the expansive nature of gypsum and ettringite, the most prominent products of sulfate attack, characterized by expansion factors ranging from 1.25 to 2.76 [4].

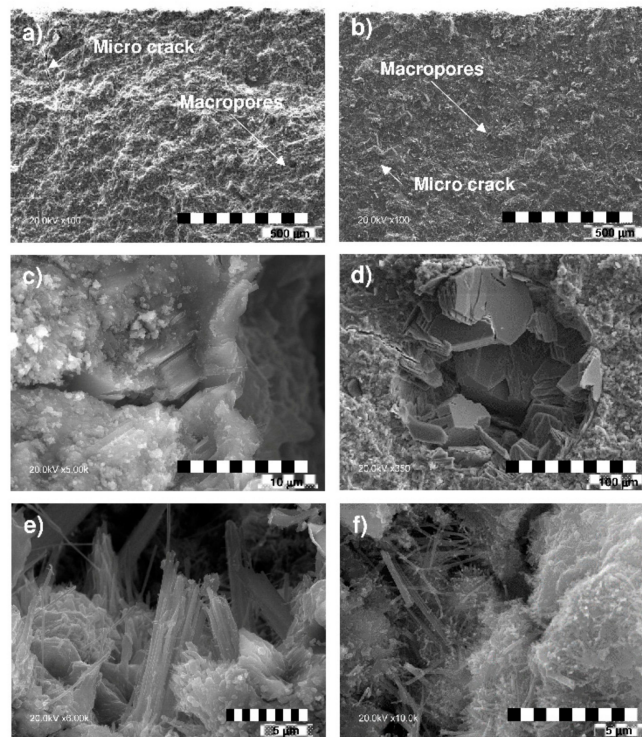


**Figure 6.** SEM micrographs of the compounds formed in cement pastes after 180 days exposure to 0.3 M  $\text{Na}_2\text{SO}_4$ : (a) OPC; (b) OPC + 20 BA; gypsum plates in (c) OPC and (d) OPC + 20 BA; and ettringite needles in (e) OPC; (f) OPC + 20 BA.

The presence of gypsum deposits resulting from the portlandite-sodium sulfate reaction are visible in Figure 6c,d, where they can be seen to have clustered primarily inside pores (Figure 6d), the sites most favorable to nucleation [42,48]. Microcracking originated in this region and subsequently extended across the matrix. Figure 6e,f, in turn, attest to the presence of ettringite, primarily in the form of elongated needles [49,50]. The micrographs provide support for the premise that ettringite forms primarily inside pores [51]. In addition to cracks, these are the sites at which it normally crystallizes, given the favorable pressure conditions and the presence of the ions required for the needles to form there [52,53].

#### 4. Conclusions

The following conclusions can be drawn from this study:

- BA-bearing paste cement resistance to sulfate attack rises with the replacement ratio. In the 180 days materials containing 20 wt% of the addition, resistance was 6.7% higher than in the OPC of the same age.
- Because the cement pastes studied, irrespective of replacement ratio, exhibited a 56 days Köch–Steinegger corrosion index of  $>0.70$ , they may be deemed sulfate resistant at the concentrations and other experimental conditions established in this study.
- The weight and volume gains induced by sulfate soaking were lower in OPC + 20 BA than in OPC pastes, the former by 20.5% and the latter by 28.5%.
- The microcracking observed in the pastes analyzed is attributable to the expansive properties of the products of sulfate attack.
- Sulfate and sodium ingress into the paste microstructure translates primarily into inside-pore ettringite formation and gypsum plate precipitation, densifying the cementitious matrix.
- Gypsum and ettringite form primarily within the pore system, inducing its refinement.

**Author Contributions:** Conceptualization, J.M.M., M.I.S.d.R. and C.M.; methodology, J.M.M., I.F.S.d.B. and M.F.; formal analysis, J.M.M. and I.F.S.d.B.; resources, M.I.S.d.R., M.F. and C.M.; writing—original draft preparation, J.M.M. and I.F.S.d.B.; writing—review and editing, M.F., M.I.S.d.R. and C.M.; supervision, I.F.S.d.B.; project administration, M.I.S.d.R. and C.M. All authors have read and agreed to the published version of the manuscript.

**Funding:** This research was funded by the Spanish Ministry of Economy and Competitiveness (BIA2016-76643-C3-1-R) (MINECO/ERDF), as well as by the Government of Extremadura and the European Regional Development Fund (ERDF) under grant GR 18122 awarded to the MATERIA research group.

**Acknowledgments:** The cement supplied by the Lafarge Group plant Villaluenga de la Sagra, Toledo, Spain, is gratefully acknowledged.

**Conflicts of Interest:** The authors declare no conflict of interest.

#### References

1. Sun, D.; Wu, K.; Shi, H.; Miramini, S.; Zhang, L. Deformation behaviour of concrete materials under the sulfate attack. *Constr. Build. Mater.* **2019**, *210*, 232–241. [[CrossRef](#)]
2. Ragoug, R.; Omikrine-Metalssi, O.; Torrenti, J.M.; Barberon, F.; Divet, L.; Roussel, N. *External Sulfate Attack-Influence of an Early Age Exposure, Coupling with the Cement Composition*; LNEC: Lisbon, Portugal; RILEM: Lisbon, Portugal, 2016; pp. 57–68.
3. Zhang, Z.; Zhou, J.; Yang, J.; Zou, Y.; Wang, Z. Understanding of the deterioration characteristic of concrete exposed to external sulfate attack: Insight into mesoscopic pore structures. *Constr. Build. Mater.* **2020**, *260*, 119932. [[CrossRef](#)]
4. Ikumi, T.; Segura, I. Numerical assessment of external sulfate attack in concrete structures. A review. *Cem. Concr. Res.* **2019**, *121*, 91–105. [[CrossRef](#)]
5. De Souza, D.J.; Medeiros, M.H.F.; Filho, J.H. Evaluation of external sulfate attack ( $\text{Na}_2\text{SO}_4$  and  $\text{MgSO}_4$ ): Portland cement mortars containing siliceous supplementary cementitious materials. *Rev. IBRACON Estrut. Mater.* **2020**, *13*, e13403. [[CrossRef](#)]

6. Müllauer, W.; Beddoe, R.E.; Heinz, D. *Sulfate Attack on Concrete-Solution Concentration and Phase Stability*; RILEM: Toulouse, France, 2009; pp. 18–27.
7. Juenger, M.C.; Siddique, R. Recent advances in understanding the role of supplementary cementitious materials in concrete. *Cem. Concr. Res.* **2015**, *78*, 71–80. [[CrossRef](#)]
8. Kumar Metha, P.; Monteiro, P.J.M. *CONCRETE: Microstructure, Properties and Materials*, 3rd ed.; McGraw-Hill: New York, NY, USA, 2006; p. 659.
9. Whittaker, M.; Black, L. Current knowledge of external sulfate attack. *Adv. Cem. Res.* **2015**, *27*, 532–545. [[CrossRef](#)]
10. Sanjuán, M.A.; Andrade, C.; Mora, P.; Zaragoza, A. Carbon Dioxide Uptake by Cement-Based Materials: A Spanish Case Study. *Appl. Sci.* **2020**, *10*, 339. [[CrossRef](#)]
11. Martirena, F.; Monzó, J. Vegetable ashes as Supplementary Cementitious Materials. *Cem. Concr. Res.* **2018**, *114*, 57–64. [[CrossRef](#)]
12. Medina, C.; Del Bosque, I.F.S.; Frías, M.; De Rojas, M.S. Design and characterisation of ternary cements containing rice husk ash and fly ash. *Constr. Build. Mater.* **2018**, *187*, 65–76. [[CrossRef](#)]
13. Frías, M.; Savastano, H.; Villar, E.; De Rojas, M.I.S.; Santos, S. Characterization and properties of blended cement matrices containing activated bamboo leaf wastes. *Cem. Concr. Compos.* **2012**, *34*, 1019–1023. [[CrossRef](#)]
14. González-Kunz, R.N.; Pineda, P.; Bras, A.; Morillas, L. Plant biomass ashes in cement-based building materials. Feasibility as eco-efficient structural mortars and grouts. *Sustain. Cities Soc.* **2017**, *31*, 151–172. [[CrossRef](#)]
15. Rajamma, R.; Senff, L.; Ribeiro, M.; Labrincha, J.; Ball, R.J.; Allen, G.; Ferreira, V.M. Biomass fly ash effect on fresh and hardened state properties of cement based materials. *Compos. Part B Eng.* **2015**, *77*, 1–9. [[CrossRef](#)]
16. Ohenoja, K.; Wigren, V.; Österbacka, J.; Illikainen, M. Mechanically Treated Fly Ash from Fluidized Bed Combustion of Peat, Wood, and Wastes in Concrete. *Waste Biomass Valorization* **2019**, *11*, 3071–3079. [[CrossRef](#)]
17. del Bosque, I.F.S.; de Rojas, M.I.S.; Asensio, E.; Frías, M.; Medina, C. Modelling the interfacial transition zone (ITZ) between recycled aggregates and industrial waste in cementitious matrix. In *Waste and By-Products in Cement-Based Materials*; De Brito, J., Thomas, C., Medina, C., Agrela, F., Eds.; Woodhead Publishing: Sawston, UK, 2021.
18. Carević, I.; Baričević, A.; Štirmer, N.; Šantek, B.J. Correlation between physical and chemical properties of wood biomass ash and cement composites performances. *Constr. Build. Mater.* **2020**, *256*, 119450. [[CrossRef](#)]
19. Medina, J.; Del Bosque, I.S.; Frías, M.; De Rojas, M.S.; Medina, C. Design and properties of eco-friendly binary mortars containing ash from biomass-fuelled power plants. *Cem. Concr. Compos.* **2019**, *104*, 103372. [[CrossRef](#)]
20. De Brito, J.; Argela, F. Biomass fly ash and biomass bottom ash. In *New Trends in Eco-Efficient and Recycled Concrete*; Argela, F., Cabrela, M., Morales, M., Zamorano, M., Alshaaer, M., Eds.; Elsevier BV: Amsterdam, The Netherlands, 2019; pp. 23–58.
21. Teixeira, E.; Camões, A.; Branco, F. Valorisation of wood fly ash on concrete. *Resour. Conserv. Recycl.* **2019**, *145*, 292–310. [[CrossRef](#)]
22. Medina, J.; Del Bosque, I.S.; Frías, M.; De Rojas, M.S.; Medina, C. Durability of new blended cements added with recycled biomass bottom ASH from electric power plants. *Constr. Build. Mater.* **2019**, *225*, 429–440. [[CrossRef](#)]
23. Modolo, R.C.E.; Senff, L.; Ferreira, V.M.; Tarelho, L.A.C.; Moraes, C.A.M. Fly ash from biomass combustion as replacement raw material and its influence on the mortars durability. *J. Mater. Cycles Waste Manag.* **2017**, *20*, 1006–1015. [[CrossRef](#)]
24. Medina, J.M.; del Bosque, I.F.S.; Frías, M.; De Rojas, M.I.S.; Medina, C. Characterisation and valorisation of biomass waste as a possible addition in eco-cement design. *Mater. Struct.* **2017**, *50*, 207. [[CrossRef](#)]
25. Del Bosque, I.F.S.; Medina, J.; Frías, M.; De Rojas, M.S.; Medina, C. Use of biomass-fired power plant bottom ash as an addition in new blended cements: Effect on the structure of the C-S-H gel formed during hydration. *Constr. Build. Mater.* **2019**, *228*, 117081. [[CrossRef](#)]
26. Vassilev, S.V.; Baxter, D.; Andersen, L.K.; Vassileva, C.G. An overview of the composition and application of biomass ash. *Fuel* **2013**, *105*, 19–39. [[CrossRef](#)]
27. *Composition, Specifications and Conformity Criteria for Common Cements*; EN 197-Cement; European Committee for Standardization: Brussels, Belgium, 2011.
28. Koch, A.; Steinegger, U. A rapid test for cements for their behaviour under sulphate attack. *Zem. Kalk Gips* **1960**, *7*, 317–324.

29. Medina, G.; Del Bosque, I.F.S.; Frias, M.; De Rojas, M.I.S.; Medina, C. Sulfate Resistance in Cements Bearing Ornamental Granite Industry Sludge. *Materials* **2020**, *13*, 4081. [[CrossRef](#)]
30. Irassar, E.F. Sulfate resistance of blended cement: Prediction and relation with flexural strength. *Cem. Concr. Res.* **1990**, *20*, 209–218. [[CrossRef](#)]
31. *Test Method for Determination of Pore Volume and Pore Volume Distribution of Soil and Rock by Mercury Intrusion Porosimetry*; D 4404-84; ASTM International: West Conshohocken, PA, USA, 2004. [[CrossRef](#)]
32. De Rojas, M.; Frias, M.; Sabador, E.; Asensio, E.; Rivera, J.; Medina, C.; Julián, R. Durability and chromatic behavior in cement pastes containing ceramic industry milling and glazing by-products. *J. Am. Ceram. Soc.* **2018**, *102*, 1971–1981.
33. Frias, M.; De Rojas, M.I.S.; Rodríguez, C. The influence of SiMn slag on chemical resistance of blended cement pastes. *Constr. Build. Mater.* **2009**, *23*, 1472–1475. [[CrossRef](#)]
34. Goñi, S.; Frias, M.; Vegas, I.; Garcia, R. Sodium sulphate effect on the mineralogy of ternary blended cements elaborated with activated paper sludge and fly ash. *Constr. Build. Mater.* **2014**, *54*, 313–319. [[CrossRef](#)]
35. De Lucas, E.A.; Medina, C.; Frias, M.; De Rojas, M. Clay-based construction and demolition waste as a pozzolanic addition in blended cements. Effect on sulfate resistance. *Constr. Build. Mater.* **2016**, *127*, 950–958. [[CrossRef](#)]
36. Taylor, H.F.W. *Cement Chemistry*, 2nd ed.; Thomas Telford Publishing: London, UK, 1997.
37. Liu, K.-W.; Sun, D.; Wang, A.; Zhang, G.; Tang, J. Long-Term Performance of Blended Cement Paste Containing Fly Ash against Sodium Sulfate Attack. *J. Mater. Civ. Eng.* **2018**, *30*, 04018309. [[CrossRef](#)]
38. Ikumi, T.; Cavalaro, S.H.P.; Segura, I. The role of porosity in external sulphate attack. *Cem. Concr. Compos.* **2019**, *97*, 1–12. [[CrossRef](#)]
39. Bassuoni, M.; Rahman, M. Response of concrete to accelerated physical salt attack exposure. *Cem. Concr. Res.* **2016**, *79*, 395–408. [[CrossRef](#)]
40. Shi, Z.; Ferreiro, S.; Lothenbach, B.; Geiker, M.R.; Kunther, W.; Kaufmann, J.; Herfort, D.; Skibsted, J. Sulfate resistance of calcined clay–Limestone–Portland cements. *Cem. Concr. Res.* **2019**, *116*, 238–251. [[CrossRef](#)]
41. Tixier, R.; Mobasher, B. Modeling of Damage in Cement-Based Materials Subjected to External Sulfate Attack. I: Formulation. *J. Mater. Civ. Eng.* **2003**, *15*, 305–313. [[CrossRef](#)]
42. Santhanam, M.; Cohen, M.D.; Olek, J. Mechanism of sulfate attack: A fresh look: Part 2. Proposed mechanisms. *Cem. Concr. Res.* **2003**, *33*, 341–346. [[CrossRef](#)]
43. Santhanam, M.; Cohen, M.D.; Olek, J. Mechanism of sulfate attack: A fresh look Part 1: Summary of experimental results. *Cem. Concr. Res.* **2002**, *32*, 915–921. [[CrossRef](#)]
44. Müllauer, W.; Beddoe, R.E.; Heinz, D. Sulfate attack expansion mechanisms. *Cem. Concr. Res.* **2013**, *52*, 208–215. [[CrossRef](#)]
45. Kuzel, H.-J. Initial hydration reactions and mechanisms of delayed ettringite formation in Portland cements. *Cem. Concr. Compos.* **1996**, *18*, 195–203. [[CrossRef](#)]
46. Liu, K.; Deng, M.; Mo, L.; Tang, J. Deterioration mechanism of Portland cement paste subjected to sodium sulfate attack. *Adv. Cem. Res.* **2015**, *27*, 477–486. [[CrossRef](#)]
47. Veiga, K.; Gastaldini, A.L.G. Sulfate attack on a white Portland cement with activated slag. *Constr. Build. Mater.* **2012**, *34*, 494–503. [[CrossRef](#)]
48. Xiong, C.; Jiang, L.; Xu, Y.; Song, Z.; Chu, H.; Guo, Q.; Xiong, C.; Jiang, L.; Xu, Y.; Song, Z.; et al. Influences of exposure condition and sulfate salt type on deterioration of paste with and without fly ash. *Constr. Build. Mater.* **2016**, *113*, 951–963. [[CrossRef](#)]
49. Komatsu, R.; Mizukoshi, N.; Makida, K.; Tsukamoto, K. In-situ observation of ettringite crystals. *J. Cryst. Growth* **2009**, *311*, 1005–1008. [[CrossRef](#)]
50. Hewlett, P.C. *Lea's Chemistry of Cement and Concrete*, 4th ed.; Elsevier: London, UK, 1998; p. 1053.
51. Neville, A.M. *Properties of Concrete*, 1st ed.; Longman Scientific & Technical: New York, NY, USA, 2008; p. 844.
52. Taylor, H.; Famy, C.; Scrivener, K. Delayed ettringite formation. *Cem. Concr. Res.* **2001**, *31*, 683–693. [[CrossRef](#)]
53. Liu, Z.; Deng, D.; De Schutter, G. Does concrete suffer sulfate salt weathering? *Constr. Build. Mater.* **2014**, *66*, 692–701. [[CrossRef](#)]

**Publisher's Note:** MDPI stays neutral with regard to jurisdictional claims in published maps and institutional affiliations.



© 2020 by the authors. Licensee MDPI, Basel, Switzerland. This article is an open access article distributed under the terms and conditions of the Creative Commons Attribution (CC BY) license (<http://creativecommons.org/licenses/by/4.0/>).